Original research

Expression pattern analysis and drug differential sensitivity of cancer-associated fibroblasts in triple-negative breast cancer

Qilong Li [a,1], Mohan Li [b,1], Kexin Zheng [b], Shuang Tang [a], Shiliang Ma [a,b,*]

[a] *College of Bioscience and Biotechnology, Shenyang Agricultural University, Shenyang, Liaoning 110866, China*
[b] *College of Food Science, Shenyang Agricultural University, Shenyang, Liaoning 110866, China*

ABSTRACT

Triple-negative breast cancer (TNBC) has the characteristics of a complex molecular landscape, aggressive or high proliferation leading to poor prognosis, and behavioral heterogeneity. The purpose of the present study was to determine the spatiotemporal expression of α-smooth muscle actin (α-SMA)-positive cancer-associated fibroblasts (CAFs) at histological level in 4T1 tumors and to predict the sensitivity to 138 drugs in patients with TNBC according to α-SMA expression. The quantitative results of fibrosis showed that the volume of 4T1 tumors correlated positively with the area of tumor fibrosis. Furthermore, we divided 4T1 tumors according to the degree of fibrosis and characterized the molecular characteristics of the four regions. Finally, the difference in the signaling pathways and sensitivity to 138 drugs was analyzed in patients with TNBC according to α-SMA expression combined with The Cancer Genome Atlas (TCGA) database. The myogenesis, TGF-β, and Notch signaling pathways were upregulated and the patients with TNBC were significantly differentially sensitive to 25 drugs. The results of in vivo experiments showed that the inhibitory effect of embelin on 4T1 tumors with high α-SMA expression was greater than that on 4TO7 tumors with low α-SMA expression. At the same time, embelin significantly decreased *α-SMA* and *PDGFRA* expression in 4T1 tumors compared with the control group. Our findings add to understanding of CAF distribution in the 4T1 tumor microenvironment and its possible role in treating cancer.

Introduction

Triple-negative breast cancer (TNBC) involves pathologically deficient expression of progesterone receptor (PR), estrogen receptor (ER), and human epidermal growth factor receptor 2 (HER2) [1]. TNBC represents about 15–20% of newly diagnosed cases and its characteristics include a complex molecular landscape, aggressive/high proliferation, leading to poor prognosis and behavioral heterogeneity [2]. The host immune response leads to rapid tumor growth, including breast cancer, which further hinders focal tumor treatments, favors recurrence, and reduces the survival rate [3]. Additionally, the rapid development of TNBC can also lead to the development of internal hypoxia and subsequent necrotic core, where triple-negative tumors promote multidrug resistance (MDR) and worse prognosis [4]. However, the role of the necrotic core still requires clarification.

The important component of TNBC tumor stroma is the cancer-associated fibroblast (CAF) [5]. As CAFs express a series of cytokines, chemokines, and extracellular matrix (ECM) proteins essential for tumor architecture, growth, invasion, and metastasis [6]. In TNBC tumors, CAFs usually have similar morphology and gene expression pattern with myofibroblasts [7]. Myofibroblasts differentiate into CAFs under the action of platelet-derived growth factor (PDGF) and transforming growth factor-β (TGF-β) signaling [8,9]. When normal fibroblasts differentiate into CAFs or myofibroblasts, they obtain α-smooth muscle actin (α-SMA) expression and increase matrix metalloproteinase (MMP) secretion to enhance tumor metastasis [7]. In in *vivo* models of breast cancer, CAFs has been shown to promote breast cancer metastasis development and progression. Therefore, research on CAFs has become a hotspot in recent years [10].

A feature of TNBC as a desmoplastic tumor is the presence of a dense collagenous stroma, mainly comprised of stromal cells such as α-SMA[+] CAFs and the derived stromal components [11]. It is well known that tumor vessels are usually embedded into the tumor stroma, which is the first and major obstacle against drug entry into the tumor tissue

from the vessels [12]. In addition, the stromal network can divide the tumor mass into different compartments, confining the drug to a limited space of tumor area, and then other tumor areas can regenerate and progress [13]. Furthermore, the site where the drug accesses the tumor is also affected by the deposition of stromal cells and compact stromal deposition. Accordingly, CAFs are increasingly considered to be the primary noncancerous target for anti-tumor therapy, rather than a bystander [14].

In the present study, we carried out a detailed investigation on the disease progression in the TNBC 4T1 tumor mouse model, and divided the tumor regions according to the degree of fibrosis. We also analyzed the pathway changes and the response differences of 138 drugs in patients with TNBC with high or low α-SMA expression according to clinical data. Finally, we compared the inhibitory effect of embelin on mouse breast tumors with differential expression of α-SMA. Our research will contribute to the understanding of the distribution of the 4T1 stromal microenvironment and its potential role in cancer treatment.

Materials and methods

Establishment of 4T1 and 4TO7 breast cancer cell line culture and tumor-bearing model

We purchased the 4T1, 4T1-GFP and 4TO7 breast cancer cells from the Cell Bank of the Chinese Academy of Sciences (Shanghai, China) and the cells were cultured as described previously [15]. RPMI 1640 medium and HyClone dialyzed fetal bovine serum was separately purchased from Gibco (Grand Island, NY, USA, cat. No 11875093) and GE Healthcare (Chicago, IL, USA, cat. No SH30079.03HI). We purchased BALB/c mice (female, 6–8 old) from Changsheng Animal Resources Center (Benxi, China). The animals were kept in a specific pathogen–free animal room at Shenyang Agricultural University. For the transplantation of the 4T1 and 4TO7 cells, 2×10^5 cells were suspended in 100 μL 0.01 mol/L phosphate-buffered saline (PBS) (Solarbio, Beijing, China, cat. no. P1022) and were injected subcutaneously into the mouse fat pad of the fourth mammary gland. The 4T1 tumor bearing-mice were sacrificed at 1, 3, 5, 7, 14, and 21 days after transplantation. The tumor width (W) and length (L) were measured using calipers to monitor the total tumor volume (mm^3), which was calculated using the following formula: $L \times W^2 \times 0.4$ [16]. All animal experiments were performed according to the Declaration of Helsinki principles. Vertebrate experiments were approved by the Committee on the Ethics of Animal Experiments of Shenyang Agricultural University (Permit Number: SYXK < Liao>2020-11006).

Parameters for quantitative reverse transcriptase-PCR (qRT-PCR)

Tumor RNA extraction was performed as previously reported [15]. Briefly, RNA was extracted from 4T1 tumors using TRIzol™ (Invitrogen, cat. no. 15596026) with column DNase digestion according to the manufacturer's instructions. Complementary DNA (cDNA) was reverse-transcribed using the RevertAid First Strand cDNA Synthesis Kit (Thermo Scientific). qRT-PCR was performed under the following conditions: 95 °C at 30 s, 95 °C at 5 s, and 60 °C at 30 s for 40 cycles. The following assays were used for amplification of the genes of interest with *Mus musculus* (house mouse) as target species- *GAPDH, α-SMA, MMP2, PDGFRA, FAP,* and *TGF-β1. GAPDH* was used as endogenous control (for primer sequences, see Supplementary Table 1).

Tumor histology

The histological analysis method was consistent with that previously described [17]. Briefly, the dissected tumors were fixed overnight at 4 °C in 4% paraformaldehyde (Solarbio, cat. no. P1110) and dehydrated using an increasing ethanol gradient, and then cleared in xylene. The 5-μm tumor sections were stained with hematoxylin and eosin (HE) and observed under optical microscopy (A1 Plus, Nikon, Tokyo, Japan). Pathologists diagnosed all samples in a blind review.

Quantification of fibrosis

Sirius Red and Masson's trichrome are most frequently used to detect collagen in tissue [18]. The tumor sections (n = 3) were stained in Sirius Red for 1 h, followed by cleaning in double-distilled water. Then, the nuclei were stained with hematoxylin for 10 min, and observed under a polarizing microscope (Nikon, Japan). Similarly, the tumor sections (n = 3) were stained using a Masson's trichrome kit according to the manufacturer's instructions (Solarbio, cat. no. G1345). ImageJ (https://imagej.net/Welcome) was used to determine quantitative tumor fibrosis [19].

Tumor tissue immunohistochemistry (IHC) and immunofluorescence (IF)

Tumor tissues samples were paraffin-embedded, fixed, and sectioned as described earlier. Antigen retrieval was performed using sodium citrate (pH 6.0) via microwaving. Non-specific binding was blocked using 5% bovine serum albumin for 1 h at 37 °C, and then the samples were incubated with the following primary antibodies: α-SMA (D151012, Sangon Biotech, Shanghai; 1:100); cytokeratin 18 (D120229, Sangon Biotech; 1:250); cytokeratin 14 (D260178; Sangon Biotech; 1:50); TGF-β1 (ab92486; Abcam; 1:100); and Ki67 (ab15580; Abcam; 1:150); MMP2 (ab97779, Abcam, US; 1:250); COL2A1 (D120453, Sangon Biotech, Shanghai; 1:100); PDGFRA (D151808, Sangon Biotech; 1:150). The sections were then incubated with secondary antibodies overnight at 37 °C and detected using a horse-radish peroxidase (HRP)-conjugated compact polymer system. Diaminobenzidine (DAB) was used as the chromogen and the sections were counterstained with hematoxylin. For IF, the sections were incubated using secondary Alexa Fluor 488 or Alexa Fluor 555 conjugated antibodies. Then, the sections were sealed with DAPI (4′, 6-diamidino-2-phenylindole)-containing sealing solution and imaged (Nikon NI confocal microscope). For the negative control group, PBS was used in place of the specific primary antibody for incubation.

Pathological and molecular diagnosis of TNBC

Human Protein Atlas (HPA, http://www.proteinatlas.org/) contains antibody-based TNBC expression profiles. HPA was used to collect representative IHC images of α-SMA, cytokeratin 18, cytokeratin 14, TGF-β1, and Ki67 in patients with TNBC tissues.

The Cancer Genome Atlas (TCGA) data source

Molecular data were obtained from TCGA Project (TCGA) patients diagnosed with TNBC. Transcriptome raw count data of the TCGA-BRCA project were downloaded from the Genomic Data Commons (GDC) Data Portal (https://portal.gdc.cancer.gov) using TCGAbiolinks. Raw reads count data were normalized across samples using DESeq and ≥1 in at least 10% of the samples for downstream analysis. The patients with TNBC in TCGA were grouped according to high or low α-SMA expression (Table S2). The median α-SMA expression in the patients with TNBC was calculated in TCGA data, and α-SMA expression higher than the median was defined as high expression; otherwise, it was defined as low expression. Relapse-free survival (RFS) curves were depicted using the Kaplan–Meier method, and log-rank tests were used to compare survival curves.

Gene set variation analysis (GSVA)

The GSVA approach was the same as in a previous article [20]. TCGA data above were used for GSVA. GSVA score T-values of >5 were considered significant.

Drug response prediction associated with α-SMA expression

Drug response was predicted using a previously reported method [21]. The drug response was predicted for each sample based on the largest publicly available pharmacogenomics database, i.e., Genomics of Drug Sensitivity in Cancer (GDSC, https://www.cancerrxgene.org/). The prediction was implemented using pRRophetic [22] and prediction accuracy was evaluated by 10-fold cross-validation based on the GDSC training set.

Embelin-treated mice

The 20 mice were randomly divided into two embelin groups (4T1-embelin and 4TO7-embelin) and three control groups (healthy, 4T1, 4TO7), with four mice per group. Seven days after 4T1 transplantation, the embelin groups received daily oral embelin (CAS 550-24-3, 50 mg/kg), while the control group received saline solution instead, which continued until day 14 of transplantation. The dose of embelin in this study was based upon the previous effect of embelin on body weight gain [23] and toxicological study of embelin [24].

Statistical analysis

R version 3.6.2 was used for all statistical analyses. If the data were normally distributed, the measurement data between the two groups were compared using the independent sample t-test, and the measurement data of ≥ 3 groups were compared using Fisher's and Welch's one-way analysis of variance (Fisher's and Welch's one-way ANOVA). If the results showed that there was a significant difference, then the non-parametric test was used for comparison when the data were of skewed distribution. The data between the two groups were measured using the nonparametric Mann-Whitney test. The screening criterion used was a p-value of < 0.05.

Results

Analysis of α-SMA expression/expression distribution and fibrosis in mouse 4T1 tumor based on time gradient

α-SMA and fibrosis are usually used as biomarkers to represent CAFs in tumor tissues. To clarify the contribution of α-SMA expression and fibrosis content to the volume of 4T1 tumors in mice, the mice were sacrificed and analyzed on days 1, 3, 5, 7, 14, and 21 after primary transplantation (Fig. 1A). HE staining showed that the transplanted 4T1 cells were randomly implanted into mouse mammary gland tissue on day 1, but an outer layer of myoepithelial cells (MECs) of mammary gland epithelium proliferated significantly compared with the healthy mammary gland. There were significantly more fibroblasts in the 4T1 tumor tissue on day 3 than on day 1, and fibroblasts infiltrated progressively until day 21, indicating that
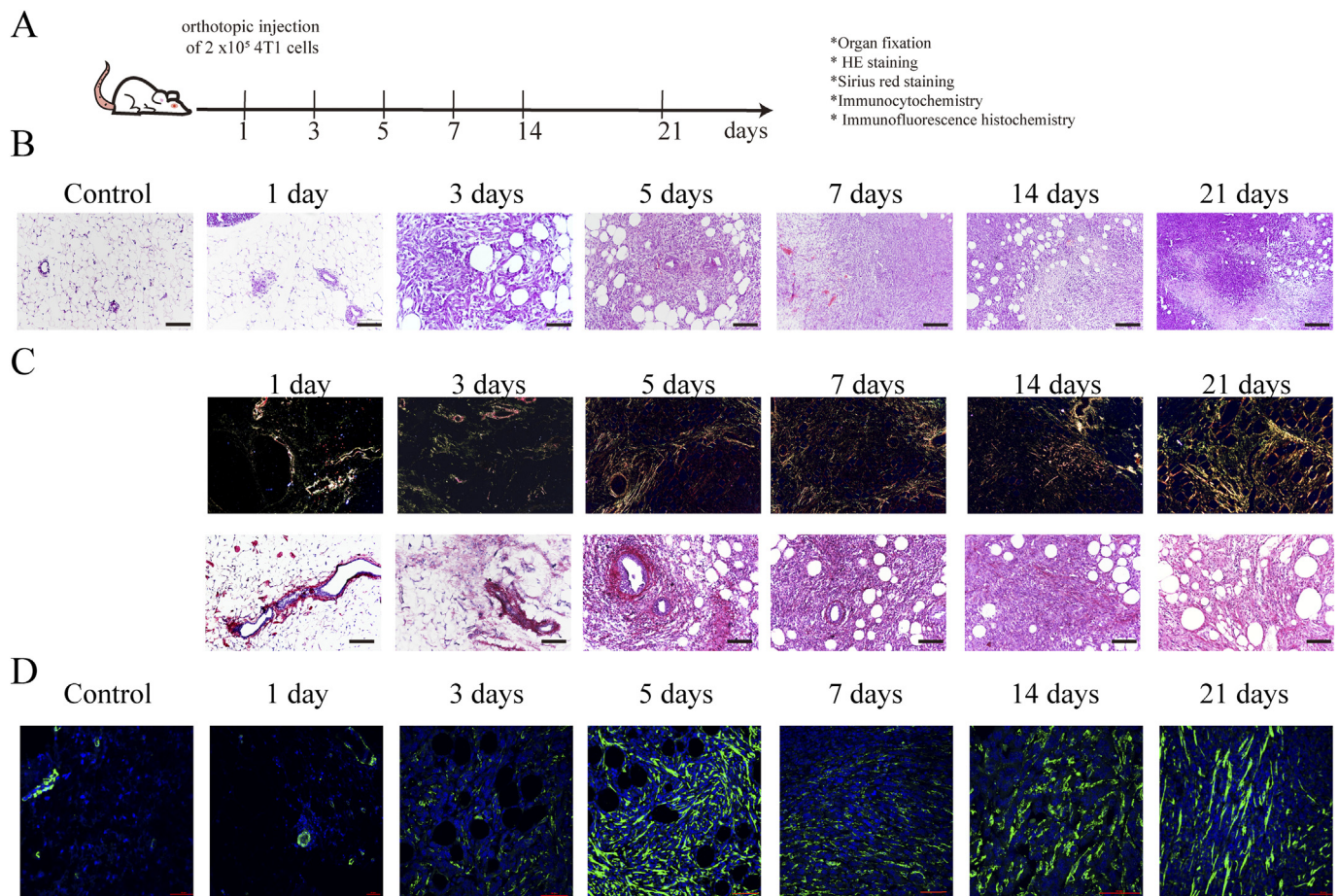
Fig. 1. Quantitative 4T1 tumor tissue fibrosis and α-SMA area. (A) Experimental design. The 4T1 bearing-mice were sacrificed at 1, 3, 5, 7, 14 and 21 days after transplantation. (B) H&E stained sections from 4T1 tumors were harvested at different times post-tumor transplant. Scale = 100 μm. (C) Sirius Red stained sections from 4T1 tumors were harvested at different times post-tumor transplant. Scale = 100 μm. (D) Immunofluorescence histochemistry for cancer associated fibroblast cells marker α-SMA on sections from 4T1 tumors were harvested at different times post-tumor transplant. Scale = 50 μm. Control = mouse without tumor transplant.

fibroblasts play a key role in tumor cell expansion and tumor development (Fig. 1B). We also measured the fibrosis area of the tumor tissue at different developmental times. The amount of fibrosis in the tumor tissue on day 3 (1.03 ± 0.13%) was significantly higher than that on day 1 (3.03 ± 0.42%, p < 0.05). The fibrosis area in tumor tissue increased until it peaked on day 21 (25.83 ± 0.93%, Fig. S1). Bright-field microscopy showed that the fibrosis surrounded the tumor cells (Fig. 1C). α-SMA was used to quantify CAFs, and the results were consistent with that of Sirius Red and HE staining (Fig. 1D). On day 1, compared to the healthy control, most of the α-SMA$^+$ cells were concentrated in the MECs but also around the adipose tissue, indicating that the 4T1 tumor cells stimulated a part of the α-SMA$^+$ CAFs. This significant increase in α-SMA$^+$ CAFs was also observed on day 3 (8.96 ± 0.63%) vs. day 1 (1.02 ± 0.12%, p < 0.05) and on day 7 (20.85 ± 2.87%) vs. day 5 (10.69 ± 0.97%, p < 0.05) (Fig. S2). Pearson's correlation coefficient showed that the correlation coefficients between the amount of fibrosis and the area of α-SMA$^+$ CAFs and tumor volume were 0.9722 (p < 0.05) and 0.9075 (p < 0.05), respectively (Fig. S3). The qRT-PCR results of α-SMA were consistent with that of IF, but the qRT-PCR results showed that α-SMA expression on day 14 was significantly higher than that on day 7 after transplantation, while the IF results were not significant (Fig. 2P). Due to the heterogeneity of the CAFs, more known CAF markers were detected by IHC and qRT-PCR. The IHC results showed that the expression of COL2A1 (Fig. 2A–E), PDGFRA (Fig. 2F–J), and MMP2 (Fig. 2K–O) in tumor tissue increased significantly with time since transplantation. Meanwhile, the qRT-PCR results for PDGFRA (Fig. 2R) and MMP2 (Fig. 2Q) were consistent with that of IHC. The qRT-PCR showed that FAP expression increased significantly from 1 day to 14 days after transplantation (Fig. 2S); TGF-β expression increased significantly from 1 day to 7 days after transplantation (Fig. 2T). The above results show that

CAFs were enriched in the tumor microenvironment in the early stage of the 4T1 tumor, suggesting that, in 4T1 tumor, CAFs are more important for early development rather than late development.

α-SMA is co-expressed with cytokeratin 14 rather than cytokeratin 18 in the 4T1 transplantation model

The 4T1-GFP cell line was used to determine whether the 14$^+$ MECs were derived from the expansion of transplanted 4T1 cells. The IF results showed that cytokeratin 14$^+$ MECs and GFP (green fluorescent protein) were not co-labeled in tumor tissue, indicating that the cytokeratin 14$^+$ MECs did not originate from tumor cells (Fig. 3A). In the mouse mammary glands, α-SMA$^+$ and cytokeratin 14$^+$ co-labeling in MECs was only detected beneath the luminal cells. However, in 4T1 tumor tissues, α-SMA$^+$ and cytokeratin 14$^+$ MEC proliferation was observed in tumor tissues and first appeared on day 7 (Fig. 3B). Meanwhile, GFP$^+$ and cytokeratin 18$^+$ double-positive 4T1 cells were restricted to the luminal cells, and most GFP$^+$ 4T1 cells were negative for cytokeratin 18 expression on day 1 (Fig. 3C). In contrast, on day 7 of tumor transplantation, most of the tumor cells were cytokeratin 18$^+$ and were not co-labeled with α-SMA (Fig. 3D).

The spatial expression patterns of α-SMA, fibrosis, cytokeratin 18, and cytokeratin 14 in 4T1 tumors

Primary 4T1 tumors exhibit typical stromal progression with inner necrotic region development. At present, 4T1 tumor tissue is divided into three regions: proliferative region, transition border, and
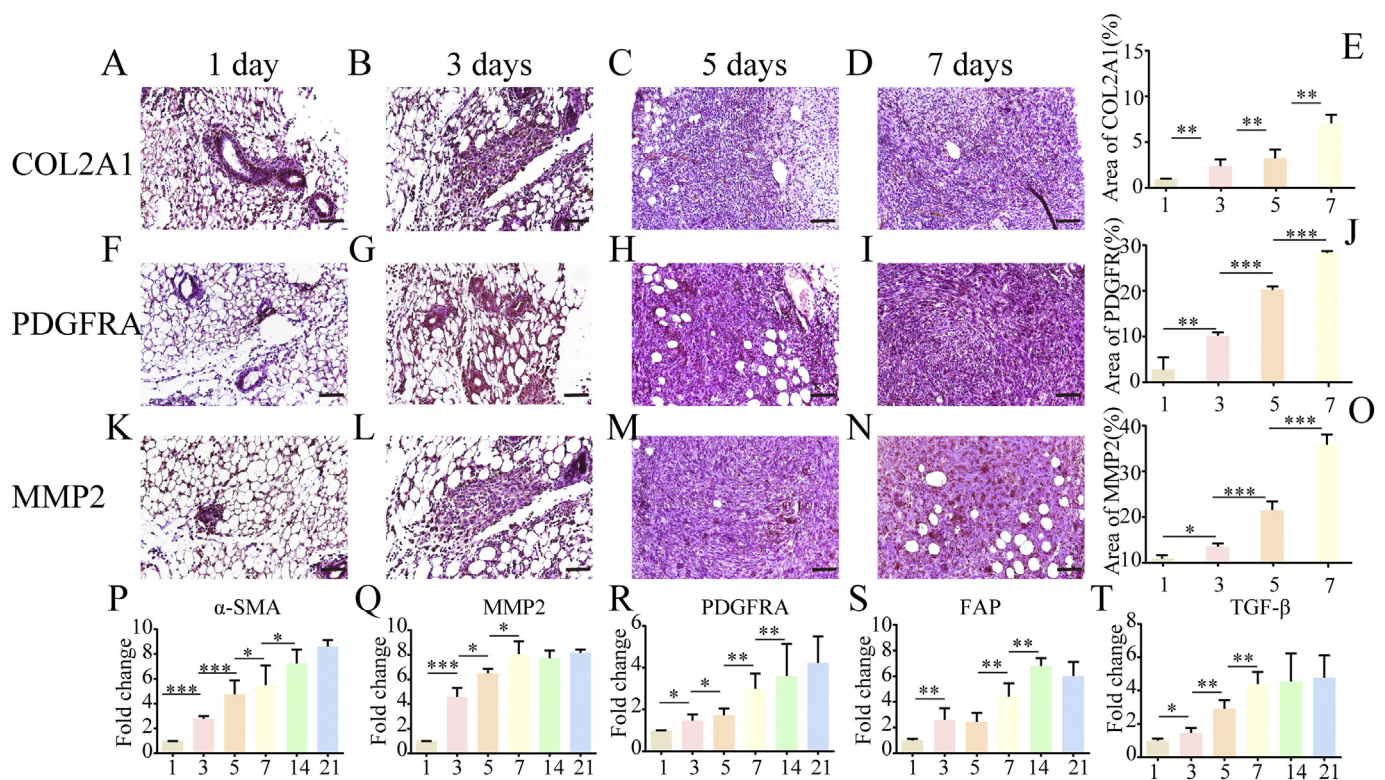
Fig. 2. Quantitative 4T1 tumor tissue CAFs. (A-E) IHC for cancer associated fibroblast cells marker COL2A1 on sections from 4T1 tumors were harvested at different times post-tumor transplant. (F-J) IHC for cancer associated fibroblast cells marker PDGFRA on sections from 4T1 tumors were harvested at different times post-tumor transplant. Scale = 100 μm. (KO) IHC for cancer associated fibroblast cells marker MMP2 on sections from 4T1 tumors were harvested at different times post-tumor transplant. Scale = 100 μm. qRT-PCR analysis of α-SMA(P), MMP2(Q), PDGFRA(R), FAP(S), and TGF-β (T) expression. * indicates that the p value is less than 0.05. ** indicates that the p value is less than 0.01. *** indicates that the p value is less than 0.005. These results have shown an average of ±SEM.
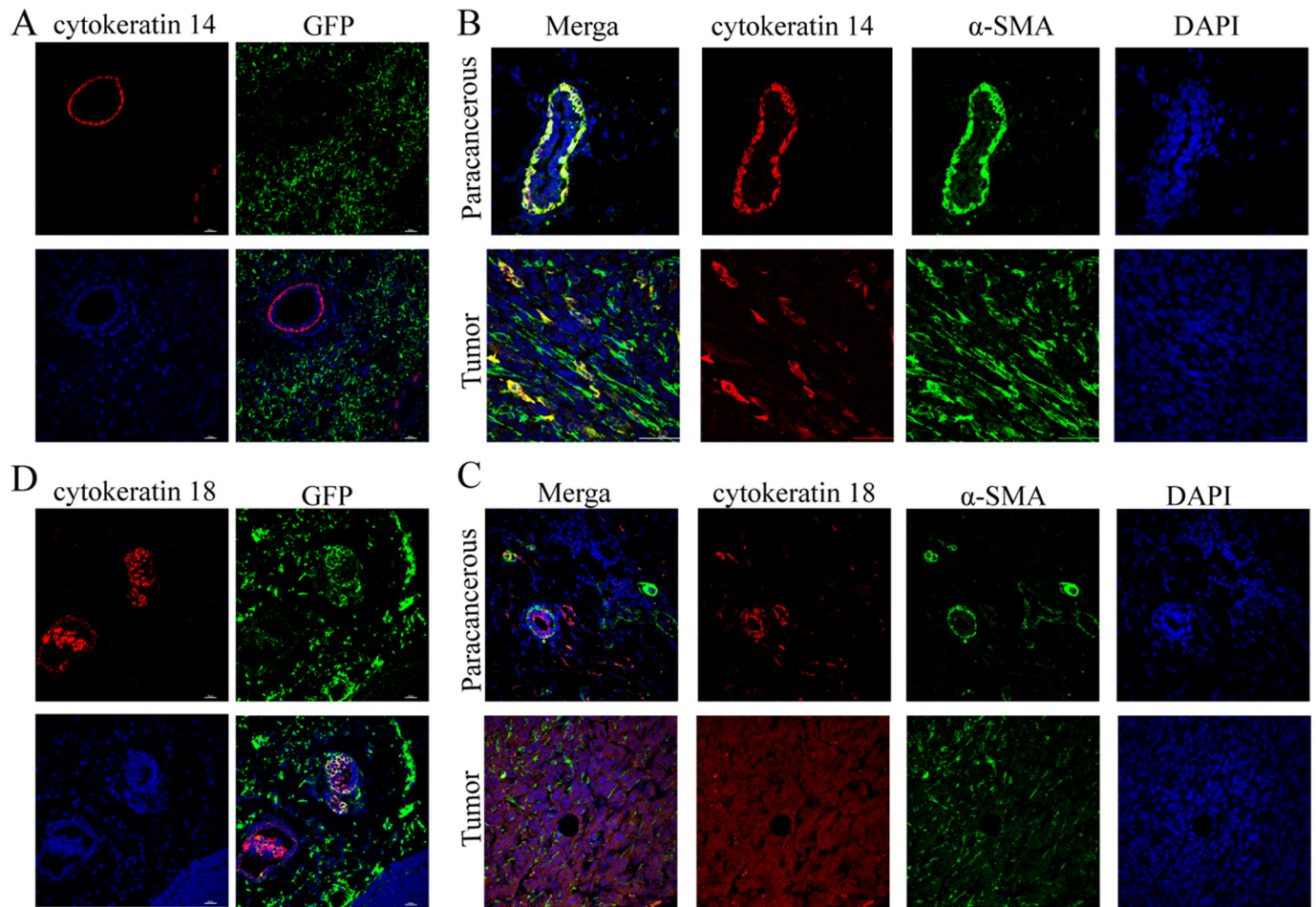
Fig. 3. Immunofluorescence histochemical analysis of cancer-associated myoepithelial cells in 4T1 tumor. (A) The images show myoepithelial cells non-co-labeled with α-SMA (Red) and GFP (Green) on the first day of tumor transplantation. Blue = DAPI. (B) The images show cancer-associated myoepithelial cells co-labeled with α-SMA and cytokeratin 14 on the 7 day of tumor transplantation. Blue = DAPI. (C) The images show luminal cells co-labeled with α-SMA and cytokeratin 18 on the first day of tumor transplantation. Blue = DAPI. (D) The images show luminal cells co-labeled with α-SMA and cytokeratin 18 on 7 day of tumor transplantation. Blue = DAPI. Scale = 20 μm. Paracancerous = Breast tissue adjacent to the tumor. (For interpretation of the references to colour in this figure legend, the reader is referred to the web version of this article.)

necrotic core [25]. According to the degree of fibrosis, the tumors were divided into pre-fibrotic region (Fig. 4A), transition border (Fig. 4B), fibrotic core (Fig. 4C), proliferative region (Fig. 4D), and para-cancerous region (Fig. 4E). Cytokeratin 18^+ cells were widely distributed in various regions of the 4T1 tumor tissues. The area of cytokeratin 14^+ cells ($0.58 \pm 0.05\%$) was significantly smaller than that of cytokeratin 18^+ cells ($89.63 \pm 0.05\%$, $p < 0.001$). Most of the cytokeratin 14^+ cells were distributed in pre-fibrotic regions ($1.68 \pm 0.25\%$), with a few being distributed in the fibrotic core ($0.08 \pm 0.05\%$) and proliferative region ($0.12 \pm 0.12\%$, $p > 0.05$). These results indicated that cytokeratin 14^+ cells might play an important role in the progression of tumor fibrosis. The area of α-SMA$^+$ CAFs was largest in the fibrotic core ($46.23 \pm 1.15\%$), followed by that in the proliferative region ($15.23 \pm 2.85\%$) and pre-fibrotic region ($23.23 \pm 6.85\%$), and was the least in the transition border region ($3.23 \pm 0.23\%$). The Masson's trichrome staining results were consistent with that of IHC of α-SMA. Fig. 3E shows the area of the 4T1 tumor bordered adipose tissue, within which cytokeratin 14^+ cells could not be found, but the MECs were cytokeratin 14–positive. In addition, most tumor cells were also cytokeratin 18–positive. Further analysis of the data showed that α-SMA$^+$ cells also infiltrated around the tumor, but fibrosis staining was negative around the MECs.

Correlation between Ki67 and α-SMA in the proliferation region

Ki67$^+$ cells were present around the α-SMA$^+$ CAFs. Ki67 was also negative in α-SMA–negative areas (Fig. 5A). TGF-β1 is a molecule that activates CAFs. We found that cytokeratin 18^+ tumor cells in the proliferation region were also labeled for TGF-β1 (Fig. 5B). Similar IHC results have been found in human TNBC. Spindle cells were present in the Ki67$^+$ tumor cells (Fig. 5C). In addition, spindle cells were usually α-SMA$^+$ cells and were abundant in the tumor tissues (Fig. 5D). Furthermore, TGF-β1 and cytokeratin 18 were only expressed in luminal epithelial cells (Fig. 5E and F).

The different expression of α-SMA in TNBC affects the activity of potential drug median inhibitory concentrations (IC_{50})

The patients with TNBC had two kinds of α-SMA expression: high and low (Fig. 6A). Patients with TNBC with high α-SMA expression had significantly shorter RFS (Fig. 6B). We identified differences in α-SMA expression, revealing the myogenesis, TGF-β1, and Notch signaling pathways (that is, the pathways associated with stem cell proliferation and differentiation) (Fig. 6C). Considering drug therapy is the common means of treating TNBC, we assessed the response of two TNBC subtypes to 138 drugs (Fig. S4). Among them, the estimated
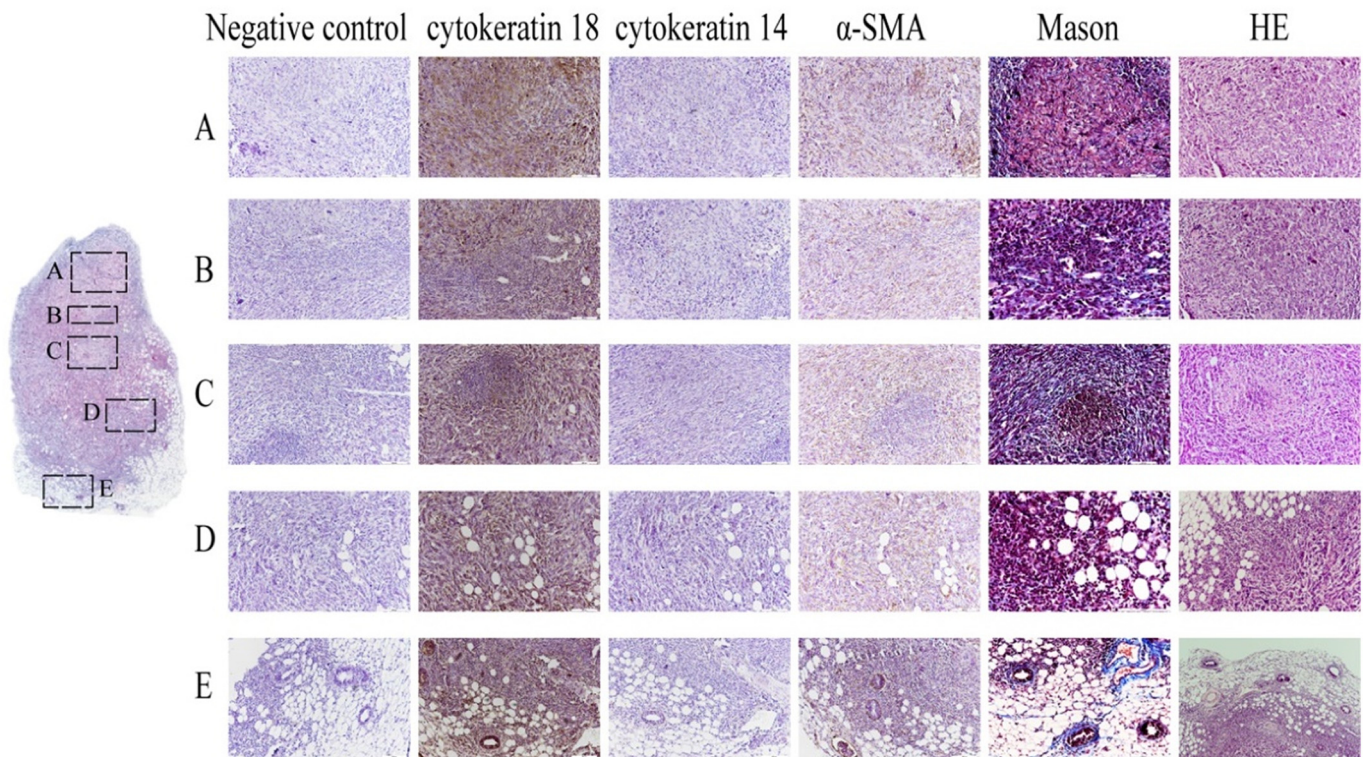
Fig. 4. Tumor regional differentiation. According to the degree of fibrosis, we divided the tumor into (A) pre-fibrotic region, (B) transition border, (C) fibrotic core and (D) proliferative region. (E) shows the area where the 4T1 tumor borders adipose tissue. The representative photos were taken at × 200 magnification. Mason = Masson's Trichrome; Negative control = the samples are incubated with only the antibody diluent without adding the primary antibody. Scale = 100 μm.

IC$_{50}$ of 24 drugs had a significant effect on α-SMA expression (p < 0.05) (Fig. S5). Rucaparib is a poly (ADP-ribose) polymerase (PARP) inhibitor used as an anti-cancer agent. α-SMA-H could be more sensitive to rucaparib (p < 0.001 and Fig. 6D). AZD6482 is an allotype selective inhibitor of phosphatidylinositol-4,5-bisphosphate 3-kinase (PI3K) p110β. However, we observed that AZD6482 presented significant response sensitivity for α-SMA-L compared with α-SMA-H (p < 0.001) (Fig. 6D). Embelin inhibits dendritic cell function and limits autoimmune encephalomyelitis through the TGF-β–β-catenin and STAT3 signaling pathways. α-SMA-H could be more sensitive to embelin (p < 0.001). To verify whether breast cancer with differential expression of α-SMA had differing embelin sensitivity, we used the α-SMA high-expression tumor 4T1 and the α-SMA low-expression tumor 4TO7 in a drug screening animal model. The inhibitory effect of embelin on 4T1 tumor volume was greater than that on the 4TO7 tumor volume (Fig. 7A). At the same time, HE staining showed that embelin induced apoptosis in 4T1 tumors (Fig. 7B). Following embelin treatment, qRT-PCR showed significantly lower *α-SMA* and *PDGFRA* levels in tumor tissue than in the control group (Fig. 7C and D), indicating that there may be less CAF infiltration in 4T1 tumor tissue.

Discussion

The tumor stromal microenvironment is very important for TNBC occurrence and development, and it is also the first line of defense of tumor drug resistance [26]. In the present study, we report the exhaustive characterization of relevant TNBC 4T1 mouse models regarding α-SMA spatiotemporal expression levels, cancer-associated MECs, and tumor division according to the degree of fibrosis, paying particular attention to the differential signaling pathways and different drug responses in patients with TNBC with high or low α-SMA expression.

The 4T1 model is the closest preclinical animal model to human TNBC [27]. The model is characterized by dense masses with mild anemia, thrombocytosis, and reticulocytosis in the short-term, and acute leukemia reaction with lymphocytosis and complement system activation in the medium- and long-term [25]. Here, we supplemented the accumulation of tumor fibrosis and α-SMA$^+$ cells to the characteristics of the 4T1 tumor. The quantitative results of fibrosis showed that 4T1 tumors began to accumulate fibrosis and α-SMA$^+$ cells as early as day 1 of transplantation, and increased significantly from day 3 onwards. Interestingly, Reigstad et al. reported that 4T1 tumors displayed increased fibrosis levels and α-SMA$^+$ cells [28], similar to the findings in our 4T1 primary tumor. Meanwhile, de Aguiar Ferreira also found that 4T1 displayed high level collagen I and α-SMA levels, as detected by IHC [29]. At present, research on α-SMA–targeting drugs based on the 4T1 model is increasing by the day [30]. Our study also provides a data basis for studying SMA targeted drugs. However, using α-SMA as the sole marker will not identify all CAFs [31]. Therefore, we will use multiple markers to study specific CAF subsets in future studies.

4T1 is a highly aggressive tumor model of malignant breast cancer in mice [32]. MECs are present in the mammary gland [33]. They form a major population around the acini and ducts [34]. In the pathological diagnosis of breast cancer, the existence of the MEC layer is a pathological hallmark of benign breast disease [34]. In general, the transplanted mouse model pays little attention to MEC function and localization, while much previous research into MECs has focused on the spontaneous tumor model, for example, MMTV-PyMT, where MECs exist in the tumor tissue as cells that limit tumor metastasis [35]. In the present article, these observations suggest that the origin
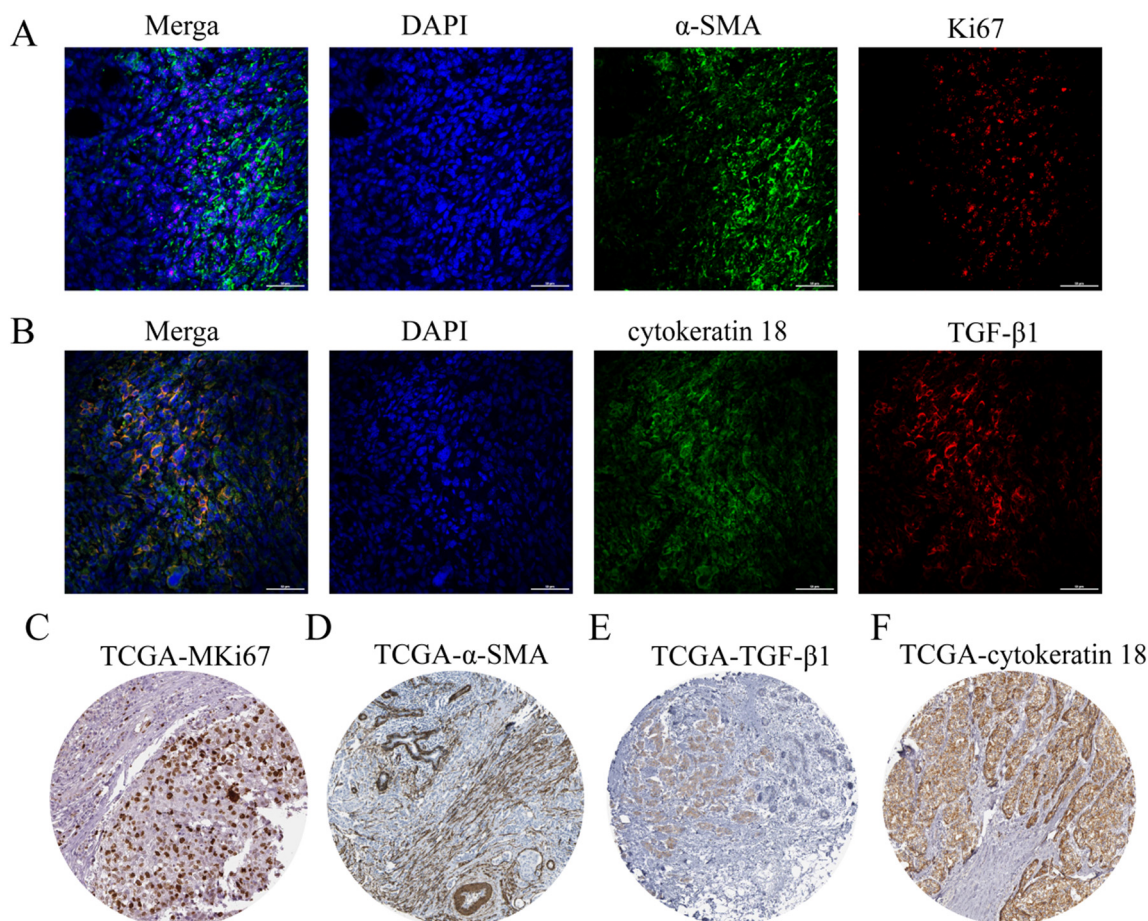
Fig. 5. Representative immunofluorescence histochemistry of 4T1 tumors and tumor tissues of patients with triple negative breast cancer. (A) Immunofluorescence histochemistry staining for α-SMA (green) and ki67 (red) in 4T1 tumors at 7 days after transplantation. (B) Immunofluorescence histochemistry staining for cytokeratin18 (green) and TGF-β1 (red) in 4T1 tumors at 7 days after transplantation. Representative images of MKi67 (C), α-SMA (D), TGF-β1 (E) and cytokeratin18 (F) in TNBC tissues were obtained from the Human Protein Atlas. The representative photos were taken at × 400 magnification. Scale = 50 μm. (For interpretation of the references to colour in this figure legend, the reader is referred to the web version of this article.)

of MECs in 4T1 tumor may be non-neoplastic cells rather than tumor cells, and provide a location for the 4T1 tumor cell enrichment. One interesting finding is that the MECs were enriched in the pre-fibrotic region and were arranged in an orderly manner. The pre-fibrotic region is a region where tumor cells are loosely arranged and extracellular fibers are enriched, into which a variety of immune cells infiltrate. According to these data, we can infer that the pre-fibrillated area is the excessive state from the tumor tissue to the fibrous core based on the gradient transplantation time. In addition, further research should be interpreted with caution to investigate the specific function of the cancer-associated MECs.

PARP1 inhibitors, such as rucaparib, are used to treat TNBC or ovarian cancer with BRCA1 or BRCA2 deletion [36]. However, patients may have different sensitivities to PARP1 inhibitor treatment, and different treatment options are needed. Therefore, finding a factor with different rucaparib sensitivity has become a research hotspot in clinical practice. In the present study, patients with TNBC with low α-SMA expression were found less sensitive to rucaparib. In addition, compared to the patients with low α-SMA expression, patients with high α-SMA expression had downregulated DNA repair, E2F TARGETS, and MYC TARGETS signaling pathways, which also participate in the activation of BRCA1. These results reflect that of Fang et al. who also found that TP53-induced glycolysis and apoptosis regulator knockdown enhanced sensitivity to PARP1 inhibitor in cancer cells by downregulating BRCA1 and the DNA repair, E2F TARGETS, and MYC

TARGETS signaling pathways [37]. As 4T1 tumors express low levels of PARP1, they are resistant to rucaparib [37]. Our results agree with that of previous studies reporting that rucaparib induces apoptosis in α-SMA$^+$ fibroblasts and represses MMP1 and MMP2 expression [38].

X-linked inhibitor of apoptosis protein (XIAP) is an anti-apoptotic protein that mainly inhibits caspase-3 activation. Therefore, the inhibition of XIAP expression may promote apoptosis [39]. As a prototypical XIAP inhibitor, embelin is widely used in TNBC treatment together with chemotherapeutic drugs [40]. Furthermore, combinations of XIAP and PARP inhibitors have an increased effect on apoptosis in the MDA-MB-231 cell line by at least two times compared with each individual inhibitor [41]. In the present study, patients with TNBC with low α-SMA expression were less sensitive to embelin. In addition, compared to the patients with low expression, patients with high α-SMA expression had upregulation of the TGF-β signaling pathway, IL-6–JAK–STAT3 pathway, and the myogenesis signaling pathway, all of which also participate in α-SMA activation. Those observations and ours are further exemplified in the work by Coutelle et al., who revealed that the impaired development of vascularized granulation tissue in embelin-treated animals was associated with a significant reduction in α-SMA–stained myofibroblasts [42]. Embelin inhibits dendritic cell function and limits autoimmune encephalomyelitis through the TGF-β–β-catenin and STAT3 signaling pathways [43]. This may be one reason the patients with TNBC with different α-SMA expression levels had different sensitivities to embelin.
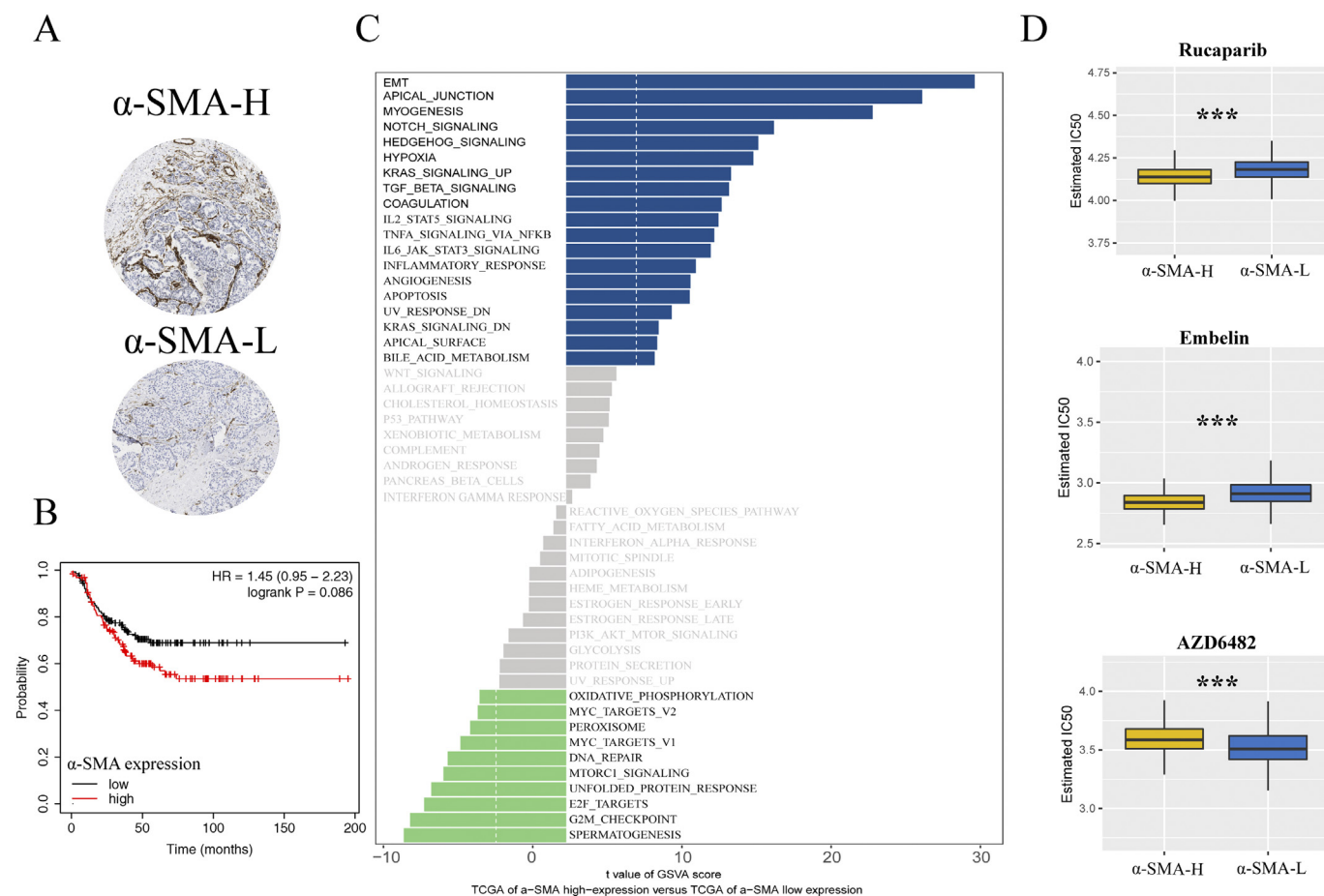
Fig. 6. GSVA and drugs response prediction associated with α-SMA expression (A) Representative images of different α-SMA expression in TNBC tissues were obtained from the Human Protein Atlas. α-SMA-H = TNBC patients with high expression of α-SMA, α-SMA-L = TNBC patients with low expression of α-SMA. (B) Kaplan–Meier plots for relapse-free survival. (C) Differences in pathway activities scored by GSVA between TNBC patients with high expression of α-SMA and low expression of α-SMA. Shown are t values from a linear model, corrected for patient of origin. DN = down; UV = ultraviolet; v1 = version v2 = version 2; EMT = Epithelial mesenchymal transition. The box plots of the estimated IC$_{50}$ for rucaparib, embelin and AZD6482 are shown in (D) for α-SMA–based α-SMA-H and α-SMA-L. ***p < 0.001.

One of the most crucial differences between AZD6482 and the two drugs above is that patients with TNBC with low α-SMA expression were highly sensitive to AZD6482. AZD6482, an allotype selective inhibitor of PI3K p110 β, is used in combination with PARP inhibitor for treating TNBC [44]. AZD6482 alone had no inhibitory effect on the MDA-MB-231 cell line. However, AZD6482 had an obvious inhibitory effect on a 3D MDA-MB-231 tumor culture model [44]. Lastly, these results show that patients with TNBC can be further stratified by α-SMA expression–based drug sensitivity prediction.

Conclusion

The purpose of the present study was to determine the spatiotemporal expression of α-SMA$^+$ CAFs at histological level in 4T1 tumors and to predict the sensitivity to 138 drugs in patients with TNBC according to α-SMA expression. Our results showed that α-SMA$^+$ CAFs started to proliferate on day 3 after transplantation, and based on α-SMA level and fibrosis area, there was progressive formation of four different histological regions in the 4T1 tumor. Furthermore, this study represents a comprehensive examination of 4T1 tumor fibrosis at different times of transplantation. However, the generality of our results is limited. For example, α-SMA–positive status does not represent all CAF subgroups. In addition, the corresponding clinical data we employed and collated are limited to TCGA data and literature. In summary, our present study increases our understanding of 4T1 tumor fibrosis and differential drug sensitivity in patients with TNBC.

CRediT authorship contribution statement

Qilong Li: Conceptualization, Validation, Writing- Original Draft, Visualization. **Mohan Li**: Investigation, Writing- Original Draft, Visualization. **Kexin Zheng**: Visualization, Investigation. **Shuang Tang**: Software, Validation. **Shiliang Ma**: Conceptualization, Supervision, Project Administration, Funding Acquisition, Writing- Review and Editing.

Declaration of competing interest

The authors declare that they have no known competing financial interests or personal relationships that could have appeared to influence the work reported in this paper.
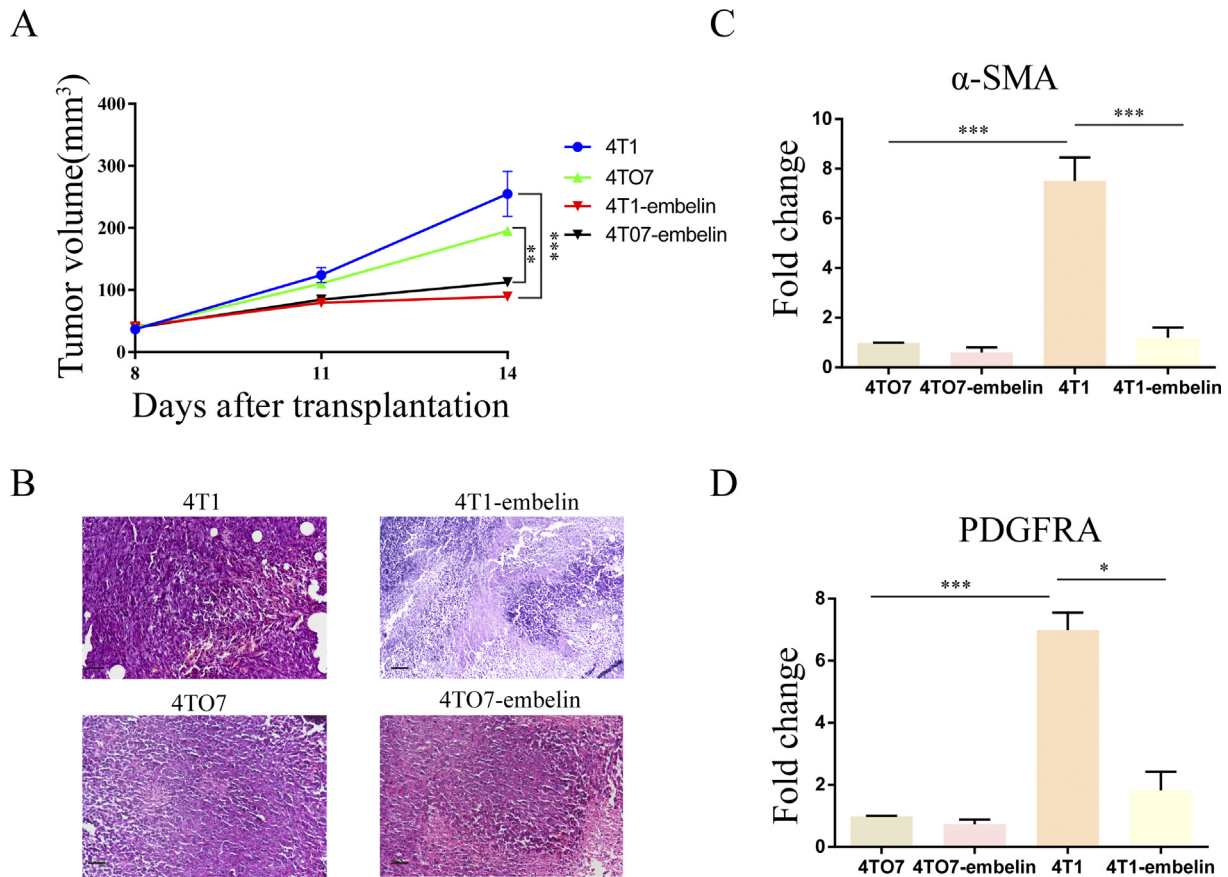
Acknowledgements

Appendix A. Supplementary data

Supplementary data to this article can be found online at https://doi.org/10.1016/j.tranon.2020.100891.

A

B

C

D

Fig. 7. The differential inhibition between 4T1 and 4TO7 tumor. (A) Average tumor volume curves of different groups of mice with orthotopic tumors. (B) HE in different groups. Scale = 100 μm. The mean difference was compared by *t*-test (p < 0.05). qRT-PCR analysis of α-SMA(C) and PDGFRA(D) expression. * indicates that the p value is less than 0.05. *** indicates that the p value is less than 0.005. 4T1-embelin = treatment of 4T1 mice with embelin; 4TO7-embelin = treatment of 4T1 mice with embelin. These results have shown an average of ± SEM.

References

[1] K. Aysola, A. Desai, C. Welch, J. Xu, Y. Qin, V. Reddy, R. Matthews, C. Owens, J. Okoli, D.J. Beech, C.J. Piyathilake, S.P. Reddy, V.N. Rao, Triple negative breast cancer - an overview, Hereditary Genet. 2013 (2013) 001.

[2] G. Bianchini, J.M. Balko, I.A. Mayer, M.E. Sanders, L. Gianni, Triple-negative breast cancer: challenges and opportunities of a heterogeneous disease, Nat. Rev. Clin. Oncol. 13 (2016) 674–690.

[3] L.M. Tseng, N.C. Hsu, S.C. Chen, Y.S. Lu, C.H. Lin, D.Y. Chang, H. Li, Y.C. Lin, H.K. Chang, T.C. Chao, F. Ouyang, M.F. Hou, Distant metastasis in triple-negative breast cancer, Neoplasma 60 (2013) 290–294.

[4] O. Brouckaert, H. Wildiers, G. Floris, P. Neven, Update on triple-negative breast cancer: prognosis and management strategies, Int. J. Women's Health 4 (2012) 511–520.

[5] J. Zhou, X.H. Wang, Y.X. Zhao, C. Chen, X.Y. Xu, Q. Sun, H.Y. Wu, M. Chen, J.F. Sang, L. Su, X.Q. Tang, X.B. Shi, Y. Zhang, Q. Yu, Y.Z. Yao, W.J. Zhang, Cancer-associated fibroblasts correlate with tumor-associated macrophages infiltration and lymphatic metastasis in triple negative breast cancer patients, J. Cancer 9 (2018) 4635–4641.

[6] G.S. Karagiannis, T. Poutahidis, S.E. Erdman, R. Kirsch, R.H. Riddell, E.P. Diamandis, Cancer-associated fibroblasts drive the progression of metastasis through both paracrine and mechanical pressure on cancer tissue, Mol. Cancer Res. MCR 10 (2012) 1403–1418.

[7] R.J. Buchsbaum, S.Y. Oh, Breast cancer-associated fibroblasts: where we are and where we need to go, Cancers 8 (2016).

[8] K. Shiga, M. Hara, T. Nagasaki, T. Sato, H. Takahashi, H. Takeyama, Cancer-associated fibroblasts: their characteristics and their roles in tumor growth, Cancers 7 (2015) 2443–2458.

[9] Y. Fuyuhiro, M. Yashiro, S. Noda, S. Kashiwagi, J. Matsuoka, Y. Doi, Y. Kato, T. Hasegawa, T. Sawada, K. Hirakawa, Upregulation of cancer-associated myofibroblasts by TGF-β from scirrhous gastric carcinoma cells, Br. J. Cancer 105 (2011) 996–1001.

[10] K. Louault, T. Bonneaud, C. Séveno, P. Gomez-Bougie, F. Nguyen, F. Gautier, N. Bourgeois, D. Loussouarn, O. Kerdraon, S. Barillé-Nion, Interactions between cancer-associated fibroblasts and tumor cells promote MCL-1 dependency in estrogen receptor-positive breast cancers, Oncogene 38 (2019) 3261–3273.

[11] T. Yu, G. Di, Role of tumor microenvironment in triple-negative breast cancer and its prognostic significance, Chin. J. Cancer Res. 29 (2017) 237–252.

[12] R.K. Jain, J.D. Martin, T. Stylianopoulos, The role of mechanical forces in tumor growth and therapy, Annu. Rev. Biomed. Eng. 16 (2014) 321–346.

[13] T. Stylianopoulos, L.L. Munn, R.K. Jain, Reengineering the physical microenvironment of tumors to improve drug delivery and efficacy: from mathematical modeling to bench to bedside, Trends Cancer 4 (2018) 292–319.

[14] Y. Zhu, F. Yu, Y. Tan, Y. Hong, T. Meng, Y. Liu, S. Dai, G. Qiu, H. Yuan, F. Hu, Reversing activity of cancer associated fibroblast for staged glycolipid micelles against internal breast tumor cells, Theranostics 9 (2019) 6764.

[15] Y. Lu, Q. Li, K. Zheng, C. Fu, C. Jiang, D. Zhou, C. Xia, S. Ma, Development of a high efficient promoter finding method based on transient transfection, Gene: X 2 (2019) 100008.

[16] D.M. Dykxhoorn, Y. Wu, H. Xie, F. Yu, A. Lal, F. Petrocca, D. Martinvalet, E. Song, B. Lim, J. Lieberman, miR-200 enhances mouse breast cancer cell colonization to form distant metastases, PLoS one 4 (2009), e7181, .

[17] Q. Li, M. Li, J. Zhang, X. Shi, M. Yang, Y. Zheng, X. Cao, X. Yue, S. Ma, Donkey milk inhibits triple-negative breast tumor progression and is associated with increased cleaved-caspase-3 expression, Food Funct. 11 (2020) 3053–3065.

[18] S. De Jong, T. van Veen, J. de Bakker, H. Van Rijen, Monitoring cardiac fibrosis: a technical challenge, Neth. Hear. J. 20 (2012) 44–48.

[19] A.M. Hadi, K.T. Mouchaers, I. Schalij, K. Grunberg, G.A. Meijer, A. Vonk-Noordegraaf, W.J. van der Laarse, J.A. Beliën, Rapid quantification of myocardial fibrosis: a new macro-based automated analysis, Cell. Oncol. 34 (2011) 343–354.

[20] D. Lambrechts, E. Wauters, B. Boeckx, S. Aibar, D. Nittner, O. Burton, A. Bassez, H. Decaluwé, A. Pircher, K. Van den Eynde, Phenotype molding of stromal cells in the lung tumor microenvironment, Nat. Med. 24 (2018) 1277–1289.

[21] X. Lu, L. Jiang, L. Zhang, Y. Zhu, W. Hu, J. Wang, X. Ruan, Z. Xu, X. Meng, J. Gao, Immune signature-based subtypes of cervical squamous cell carcinoma tightly associated with human papillomavirus type 16 expression, molecular features, and clinical outcome, Neoplasia 21 (2019) 591–601.

[22] P. Geeleher, N. Cox, R.S. Huang, pRRophetic: an R package for prediction of clinical chemotherapeutic response from tumor gene expression levels, PLoS One 9 (2014).

[23] U. Bhandari, H.S. Chaudhari, A.N. Bisnoi, V. Kumar, G. Khanna, K. Javed, Anti-obesity effect of standardized ethanol extract of Embelia ribes in murine model of high fat diet-induced obesity, PharmaNutrition 1 (2013) 50–57.

[24] Y. Debebe, M. Tefera, W. Mekonnen, D. Abebe, S. Woldekidan, A. Abebe, Y. Belete, T. Menberu, B. Belayneh, B. Tesfaye, Evaluation of anthelmintic potential of the Ethiopian medicinal plant Embelia schimperi Vatke in vivo and in vitro against some intestinal parasites, BMC Complement. Altern. Med. 15 (2015) 1–6.

[25] J.J. Arroyo-Crespo, A. Armiñán, D. Charbonnier, C. Deladriere, M. Palomino-Schätzlein, R. Lamas-Domingo, J. Forteza, A. Pineda-Lucena, M.J. Vicent, Characterization of triple-

negative breast cancer preclinical models provides functional evidence of metastatic progression, Int. J. Cancer 145 (2019) 2267–2281.

[26] Mirjam C. Boelens, Tony J. Wu, Barzin Y. Nabet, B. Xu, Y. Qiu, T. Yoon, Diana J. Azzam, C. Twyman-Saint Victor, Brianne Z. Wiemann, H. Ishwaran, Petra J. ter Brugge, J. Jonkers, J. Slingerland, Andy J. Minn, Exosome transfer from stromal to breast cancer cells regulates therapy resistance pathways, Cell 159 (2014) 499–513.

[27] B.A. Pulaski, S. Ostrand-Rosenberg, Mouse 4T1 breast tumor model, Current Protocols in Immunology 39 (2000) (20.22. 21-20.22. 16).

[28] I. Reigstad, H.Y. Smeland, T. Skogstrand, K. Sortland, M.C. Schmid, R.K. Reed, L. Stuhr, Stromal integrin α11β1 affects RM11 prostate and 4T1 breast xenograft tumors differently, PLoS One 11 (2016).

[29] C. de Aguiar Ferreira, Radiolabeled Moieties for Molecular Imaging and Cancer Theranostics, The University of Wisconsin-Madison, 2019.

[30] M. Murakami, M.J. Ernsting, E. Undzys, N. Holwell, W.D. Foltz, S.-D. Li, Docetaxel conjugate nanoparticles that target α-smooth muscle actin–expressing stromal cells suppress breast cancer metastasis, Cancer Res. 73 (2013) 4862–4871.

[31] H. Sugimoto, T.M. Mundel, M.W. Kieran, R. Kalluri, Identification of fibroblast heterogeneity in the tumor microenvironment, Cancer Biol. Ther. 5 (2006) 1640–1646.

[32] P. Kaur, G.M. Nagaraja, H. Zheng, D. Gizachew, M. Galukande, S. Krishnan, A. Asea, A mouse model for triple-negative breast cancer tumor-initiating cells (TNBC-TICs) exhibits similar aggressive phenotype to the human disease, BMC Cancer 12 (2012) 120.

[33] S. Cristea, K. Polyak, Dissecting the mammary gland one cell at a time, Nat. Commun. 9 (2018) 1–3.

[34] K.C. Gatter, Handbook of immunohistochemistry and in situ hybridisation of human carcinomas: molecular genetics – lung and breast carcinomas, Br. J. Cancer 93 (2005) 1318.

[35] M.M. Fluck, B.S. Schaffhausen, Lessons in signaling and tumorigenesis from polyomavirus middle T antigen, Microbiology and Molecular Biology Reviews: MMBR 73 (2009) 542–563 (Table of Contents).

[36] K.E. McCann, S.A. Hurvitz, Advances in the use of PARP inhibitor therapy for breast cancer, Drugs Context 7 (2018).

[37] P. Fang, C. De Souza, K. Minn, J. Chien, Genome-scale CRISPR knockout screen identifies TIGAR as a modifier of PARP inhibitor sensitivity, Commun. Biol. 2 (2019) 1–16.

[38] T.H. Park, C.W. Kim, J.S. Choi, Y.J. Park, Y. Chong, M.J. Park, Y. Cho, PARP1 inhibition as a novel therapeutic target for keloid disease, Adv. Wound Care 8 (2019) 186–194.

[39] G. Hassanzadeh, T. Naing, T. Graber, S.M. Jafarnejad, D.F. Stojdl, T. Alain, M. Holcik, Characterizing cellular responses during oncolytic maraba virus infection, Int. J. Mol. Sci. 20 (2019) 580.

[40] E. Strekalova, D. Malin, H. Rajanala, V.L. Cryns, Metformin sensitizes triple-negative breast cancer to proapoptotic TRAIL receptor agonists by suppressing XIAP expression, Breast Cancer Res. Treat. 163 (2017) 435–447.

[41] A.K. Siraj, P. Pratheeshkumar, S.K. Parvathareddy, S.P. Divya, F. Al-Dayel, A. Tulbah, D. Ajarim, K.S. Al-Kuraya, Overexpression of PARP is an independent prognostic marker for poor survival in Middle Eastern breast cancer and its inhibition can be enhanced with embelin co-treatment, Oncotarget 9 (2018) 37319.

[42] O. Coutelle, H.T. Hornig-Do, A. Witt, M. Andree, L.M. Schiffmann, M. Piekarek, K. Brinkmann, J.M. Seeger, M. Liwschitz, S. Miwa, Embelin inhibits endothelial mitochondrial respiration and impairs neoangiogenesis during tumor growth and wound healing, EMBO Mol. Med. 6 (2014) 624–639.

[43] Z. Xue, Z. Ge, K. Zhang, R. Sun, J. Yang, R. Han, M. Peng, Y. Li, W. Li, D. Zhang, Embelin suppresses dendritic cell functions and limits autoimmune encephalomyelitis through the TGF-β/β-catenin and STAT3 signaling pathways, Mol. Neurobiol. 49 (2014) 1087–1101.

[44] N. Dey, J. Carlson, P. De, B. Leyland-Jones, Abstract P2-03-06: PTEN expression at the nexus of oncogenic signals in TNBC: testing combination of p110beta-isoform-specific inhibitor with five PARP inhibitors, Cancer Research 79 (2019) (P2-03-06-P02-03-06).